Earth and Planetary Science Letters 295 (2010) 147–158

Contents lists available at ScienceDirect

Earth and Planetary Science Letters

journal homepage: www.elsevier.com/locate/epsl

# The Lunar rayed-crater population — Characteristics of the spatial distribution and ray retention

Stephanie C. Werner *, Sergei Medvedev

*Physics of Geological Processes, University of Oslo, Norway*

ARTICLE INFO

*Article history:*
Received 2 October 2009
Received in revised form 18 March 2010
Accepted 24 March 2010
Available online 24 April 2010

Editor: T. Spohn

*Keywords:*
Moon
cratering
ray retention
spatial distribution
rate

ABSTRACT

The global statistics for young impact craters on the Moon is used to unravel potential spatial asymmetries, that may have been introduced by the particular orbital configuration of a synchronously rotating satellite. Only craters that exhibit bright ejecta rays extending for several crater radii were considered in this study. This crater population is younger than about 750 Ma. The shape of the crater size-frequency distribution does not show strong dependence on the target properties (mare vs. highlands). However, slightly lower frequencies indicate a shorter retention of the visibility of rays in mare units when their visibility is purely due to immaturity and not due to composition. Rays of small craters fade away much faster. Large, old, rayed craters sustain their visibility longer than the average crater population because of the compositional contrast between rays and mare material, and thus obscure the cratering record when investigated for spatial variations. Using the existence of rays purely based on optical maturity instead of visibility as marker horizon for the Copernican–Eratosthenian boundary, suggests a shift from 1.1 Ga to 750 Ma.

The spatial distribution of lunar rayed craters, namely the latitudinal and longitudinal frequency variations, does not agree with previous analytical and numerical studies. Although there is an apparent hemispherical asymmetry centred close to the apex, the density distribution is patchy and no predicted spatial pattern could be confirmed. Spatial distribution corrections accounting for the lower frequencies in the mare areas did not result in a better agreement with the analytical estimates. Density variations are less than 15% over vast parts of the lunar surface, and the uncertainties for absolute surface ages are similar. However, variations of up to 50% are found even for the more numerous small craters. These extreme values are located at high latitudes. A combination of crater-forming projectile flux distribution and micrometeorite bombardment, which acts on maturation of the ray systems, could prove as an explanation for the contradicting observed rayed crater distribution.

An analysis of the older craters is more challenging (on the Moon) because earlier geological processes complicate the setting, and the orbital configuration of the Moon–Earth–Sun–projectile system altered with time.



## 1. Introduction

Impact crater formation is one of the most common geological processes on the rocky bodies of the solar system and crater counts can be used to determine relative and absolute surface ages, if the crater-production rate and size-frequency distribution are known (e.g., Shoemaker et al., 1963; Hartmann, 1966; Oberbeck et al., 1977; Neukum, 1983; Ivanov, 2001). This approach assumes a random and globally uniform crater-production rate, implying an isotropic velocity distribution for the projectile population or a target body massive enough to deviate the projectiles. The orbital configuration and synchronous rotation of almost all planetary satellites suggest, however, that a satellite's surface may exhibit spatial variations of the crater-production rate. A latitudinal dependence might be found because the inclination distribution of the projectile canddates dominantly scatters around the equatorial plane (Halliday, 1964; Le Feuvre and Wieczorek, 2006, 2008; Gallant et al., 2009). A longitudinal dependence results from synchronous rotation and the relative velocity between satellite and projectile. This suggests preferential impact cratering on the leading side of the satellite (Wiesel, 1971; Wood, 1973; Shoemaker and Wolfe, 1982; Horedt and Neukum, 1984; Zahnle et al., 1998, 2001, 2003; Morota and Furumoto, 2003; Morota et al., 2005, 2008; Gallant et al., 2009). If the majority of projectiles approach the planet–satellite system with inclination close to the satellite's orbit plane, the planet could act as a gravitational lens depending on the distance between planet and satellite, causing an asymmetry between nearside and farside of the satellite. Projectiles would be focused onto the nearside of the satellite (Turski, 1962; Wiesel, 1971; Bandermann and Singer, 1973; Wood, 1973; Le Feuvre and

* Corresponding author.
*E-mail address:* Stephanie.Werner@fys.uio.no (S.C. Werner).

0012-821X/$ – see front matter © 2010 Elsevier B.V. All rights reserved.
doi:10.1016/j.epsl.2010.03.036

Wieczorek, 2005; Gallant et al., 2009). These dependencies applied to the Moon, may result in a crater-rate maximum at the apex of the orbital motion, a lower rate at the antapex, and a minimum at the poles; however no nearside–farside effect is expected. We present here a detailed analysis of the statistical characteristics and spatial distribution of lunar rayed craters in order to unravel possible cratering rate asymmetries.

Shoemaker and Hackman (1962) first described the stratigraphic relation of the ray pattern, and suggested that they, are the youngest features on the Moon, because they superpose all other terrains. Furthermore, they explained, since the ray pattern formed is by ballistic ejection from a central crater, then these craters with rays are the youngest craters on the Moon. These craters have been assigned to the Copernican System, named after the crater Copernicus (Shoemaker and Hackman, 1962). Wilhelms (1987) does not define Copernicus as the base of the system, but models proposed by Grier et al. (2001) and Hawke et al. (2004) regard Copernicus' rayed ejecta deposits as the marker horizon based on spectral information.

Scattered all over the Moon, the rayed craters constitute a group of craters that are easily recognized and least affected by other geological processes. This crater group therefore allows us to study the spatial distribution of craters on the Moon for the period in which the orbital configuration, Earth–Moon distance, and the nearside–farside situation has been similar to today's situation.

Although the formation process of crater ejecta rays is not fully understood, rays are described as filamentous, high-albedo deposits that are radial or sub-radial to fresh craters and often extend many crater radii from the parent crater (Hawke et al., 2004). Their visibility depends mainly on the state of optical maturity of the ray material; if the composition of the ray deposits differs from the surrounding terrain, they can remain visible longer, particularly in the mare units (Hawke et al., 2004). The presence of crater rays is considered as the marker to define the Copernican–Eratosthenian boundary, and the persistence of non-compositional rays has been estimated to less than about 1.1 Ga (Wilhelms, 1987).

## 2. Crater size-frequency distribution: Age, ray retention and the role of composition

To describe the spatial and size-frequency distribution of the lunar rayed-crater population we analysed the Clementine 750 nm image mosaic data on a map scale of 1:3 million, although the image data, having a nominal pixel resolution of 100 m/pixel would allow for a larger scale. Crater detection at sizes down to about 1 km in diameter is considered complete. The image data were searched for craters which exhibit rayed ejecta extending multiple crater radii with higher albedo than the surroundings. The detection of rayed craters was done by eye based on the albedo map and constrained by mineral-ratio data presented as a RGB composite image mosaic with band ratios 750 nm/415 nm shown in red (R), 750 nm/950 nm in green (G) and 415 nm/750 nm in blue (B), so that the crater ejecta rays of young craters appear in bright blue (Pieters et al., 1994). Positively identified craters were marked by their centre points and scaled by their crater diameters in a GIS system for latitudes between 70°N and 70°S. The polar regions beyond these limits were excluded from the analysis to avoid biasing due to low illumination and phase-angle changes at higher latitudes. Fig. 1 shows the crater size-frequency distribution scaled by their diameters.

A total of 1615 craters were registered with craters as small as 500 m in diameter, but only craters with diameters greater or equal to 1 km (1263 craters, out of which 273 craters are larger than 5 km in diameter) are considered here to be detected without misses. Thus, our observed diameter range extends to considerably smaller crater diameters than in earlier measurements. Previous studies focussed on the lunar farside and were restricted to crater diameters larger than 10 km or 5 km (e.g. McEwen et al., 1997; Morota and Furumoto, 2003). Others (Grier et al., 2001) investigated craters globally, but considered only craters with diameters larger than 20 km. The detection rate of rayed craters at comparable sizes in this work is about 15% lower than earlier observations and measurements (McEwen et al., 1997; Morota and Furumoto, 2003). This corresponds roughly to the uncertainties stated by McEwen et al. (1997). None of

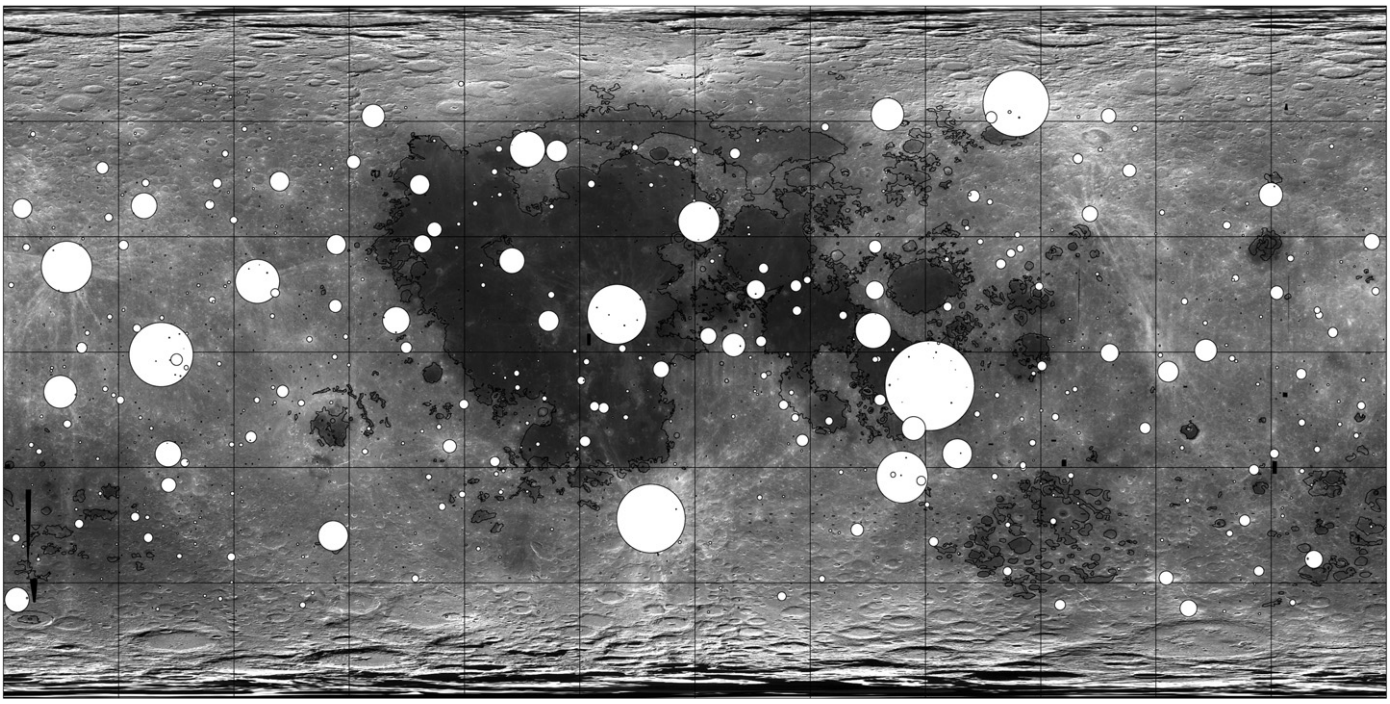

**Fig. 1.** The distribution of all rayed craters (diameters are scaled by a factor 5 for visibility, the smallest crater diameters are around 500 m) between 70°N and 70°S latitude as observed in this study on Clementine 750 nm image mosaic data on a 1:3 million map scale. The outline of mare units is shown.

the craters which McEwen et al. (1997) listed as old or questionable were considered in this study. Therefore, the set of rayed craters considered here, is a significant subset of the young craters discussed by McEwen et al. (1997), Grier et al. (2001) or Morota and Furumoto (2003). However, this study does not intend to represent all the craters of the Copernican Epoch as listed by Wilhelms et al. (1978) and discussed by McEwen et al. (1997), but to focus on a crater population that is as homogenous as possible. The cumulative crater size-frequency distribution found in this study is given in Fig. 2.

### 2.1. Age of the population and ray retention

Our age analysis is based on the standard procedure of cratering age determination with technical details described by the Crater Analysis Techniques Working Group (1979). Crater retention ages are derived by fitting a crater-production function (time-invariant crater size-frequency distribution) to the observed crater distribution. Linked to a certain reference diameter $D$ ($\geq$1 km), the cumulative crater frequency, $N_{cum}(D)$ is translated to absolute age through a cratering chronology function (describing the change in cratering rate through time). Fig. 2 shows the crater size-frequency distribution of the rayed-crater population in comparison with isochrones for 750 Ma, 1.1 Ga and 2 Ga average surface age, calculated using the crater-production function given by Ivanov (2001) and the cratering chronology function from Neukum et al. (2001).

Applied to the rayed-crater population, the crater retention age for a given segment of the rayed-crater distribution is equal to the typical retention time of rays. Hence, fitted isochrones indicate (the lower limit of) the absolute ray retention time for rays. Hawke et al. (2004) grouped lunar rays into compositional and immaturity rays, of which the latter will naturally disappear with time. Compositional rays will only disappear when the ray material is fully diluted by the surrounding material, for example due to vertical mixing or lateral transport of material from adjacent units. These processes of mixing and dilution of compositional rays take much longer than the maturation process (e.g., Pieters et al., 1985; Blewett and Hawke, 2001). The visibility of rays (their albedo contrast) in the 750 nm Clementine images can result from a combination of composition and immaturity and can be dominated by either one depending on the local circumstances. The observed deviation between the measured distribution and the idealised isochrones (Fig. 2) indicates that the retention time for the rayed-crater population is different at different diameters.

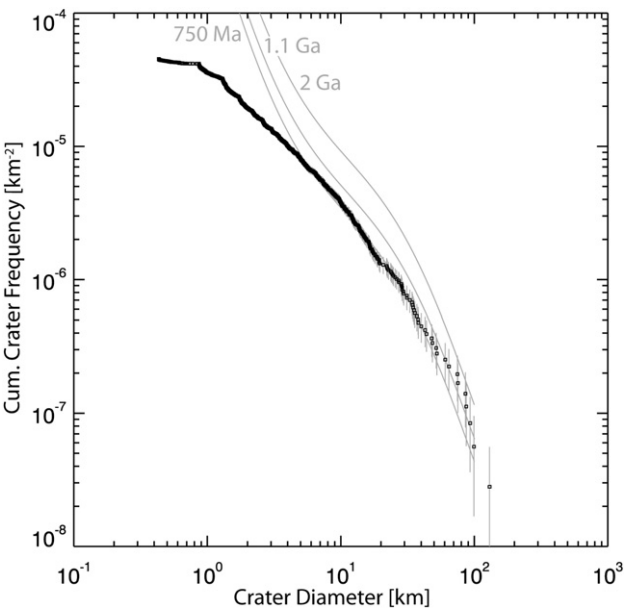


**Fig. 2.** The unbinned size-frequency distribution of rayed craters between 70°N and 70°S latitude as shown in Fig. 1. Isochrones for average surface ages of 750 Ma, 1.1 Ga (the estimated Eratosthenian–Copernican boundary) and 2 Ga are given.

The largest craters (with diameters larger than 50 km) scatter between the isochrones representing an average surface age of 2 Ga and 750 Ma, and without knowing which craters have compositional rays, we cannot determine the true maturity ray retention. The crater range between 50 km and 5 km is fitted well by the 750 Ma isochrone and yields the time which is the natural survival time of crater rays before they mature and/or dilute, and would not be recognized as rayed craters if they were older. The distribution for craters smaller than five kilometres shallows and cannot be fitted by a single isochrone. The shallower slope of the crater size-frequency distribution for small craters is due to the gradual decrease of the ray retention time with decreasing crater diameter, most likely because a smaller amount of material is involved. To resolve the small-crater distribution better, crater counts on a map scale of 1:1 million were performed for an image section shown in Fig. 3. Craters down to sizes of about 500 m in diameter are considered complete. Smaller craters (below 1 km in diameter) have an average ray retention of about five million years, given the fact that the 5 Ma isochrone represents the small-crater segment (500 m–1 km in diameter) after treating for resurfacing corrections (Werner, 2009). This is in agreement with Lucey et al. (2000a,b), who correlated optical maturity, crater sizes and age estimates, and found values indicating higher maturity on ejecta of young but smaller craters.

The age of Copernicus (diameter = 95 km), one of the most prominent bright rayed craters on the Moon, has been estimated to 800 ± 15 Ma (Stöffler and Ryder, 2001). This is slightly older than the estimated rayed crater retention time based on the global crater distribution (Fig. 2). Pieters et al. (1985) showed that the brightness of Copernicus' rays is compositional, due to the large contribution of highland material excavated from below the mare basalt at the impact site, and exhibits mature soils in places, which have not been subsequently disturbed (McCord et al., 1972a,b). Similarly, Lichtenberg, a prime example for a compositional rayed crater (Hawke et al., 2004) has been suggested to have an age of at least 1.68 Ga (Hiesinger et al., 2003). Other ages for rayed craters determined independently from isotope ratios support the pattern that compositional albedo contribution makes craters such as Autolycus (39 km, 2.1 Ga, Stöffler and Ryder, 2001) and Aristillus (55 km, 1.3 Ga, Ryder et al., 1991) stay visible, while rays due to soil immaturity are as young as 109 ± 4 Myr (Tycho, 85 km; Stöffler and Ryder, 2001), 50.3 ± 0.8 (North Ray crater, Apollo 16; Stöffler et al., 1982; Stöffler and Ryder, 2001), and 25.1 ± 1.2 (Cone crater, Apollo 14; Simon et al., 1982; Stöffler and Ryder, 2001), and are similarly bright.

### 2.2. Mare units – Composition or nearside–farside differences

McEwen et al. (1997) identified a number of large rayed craters that formed in mare units and excavated highland material from below the basaltic mare material, and therefore stay visible longer than on the highland units due to the compositional ray contrasts. One of these craters is Copernicus itself (Pieters et al., 1985). Both previous studies describe a steeper size-frequency distribution for the farside of the Moon (McEwen et al., 1997; Morota and Furumoto, 2003) than Copernican or rayed craters on the nearside as obtained by Wilhelms (1987) or Allen (1977). Moreover, the compilation of large (larger than 30 km in diameter) Copernican craters by Wilhelms (1987) is suggested to be non-random in their spatial distribution showing not only asymmetries between the near- and farside of the Moon but also within and outside the mare units.

Here, we provide a direct comparison of the rayed craters inside and outside mare units and with respect to the global distribution. Mare units were extracted from the digitised USGS Geologic Map Series of the Moon (Wilhelms and McCauley, 1971; Scott et al., 1977;

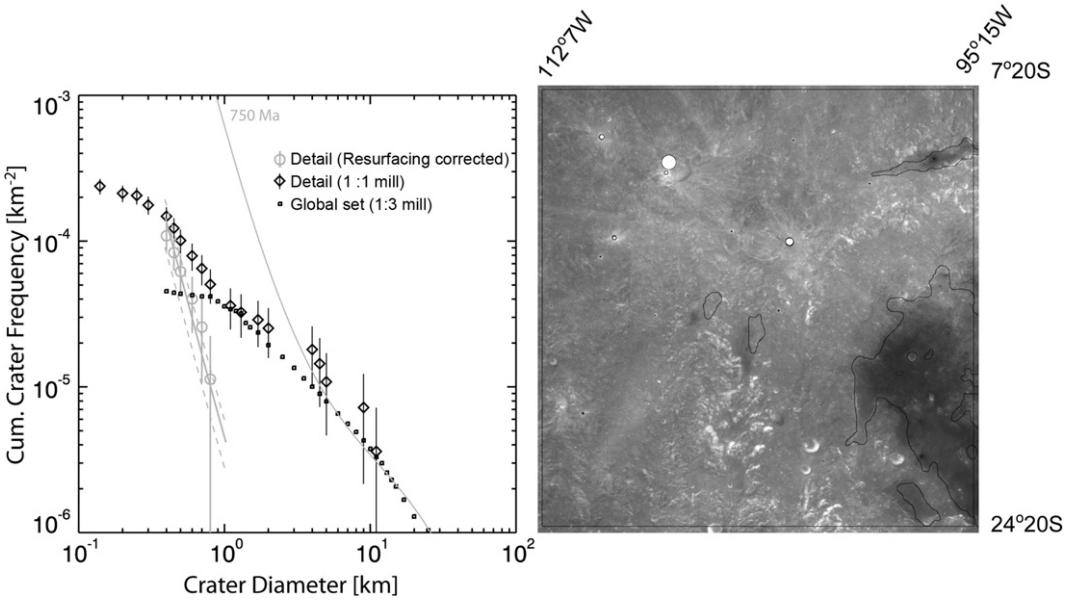


**Fig. 3.** The crater size-frequency distribution measured at 1:1 million map scale for a sub-region near Mare Orientale in comparison with the global crater size-frequency distribution (Fig. 2). After a resurfacing correction the isochrone fitting the crater size-frequency distribution is about 5 Ma indicating a ray retention of the same time for rays around craters smaller than about 1 km in diameter.

Wilhelms and El-Baz, 1977; Lucchitta, 1978; Stuart-Alexander, 1978; Wilhelms et al., 1979), and simplified (Fig. 1). Fig. 4 shows the crater size-frequency distributions for the rayed-crater population inside and outside mare units. For comparison, the total population between latitudes of 70°N and 70°S and the crater distribution found by McEwen et al. (1997) are plotted as well.

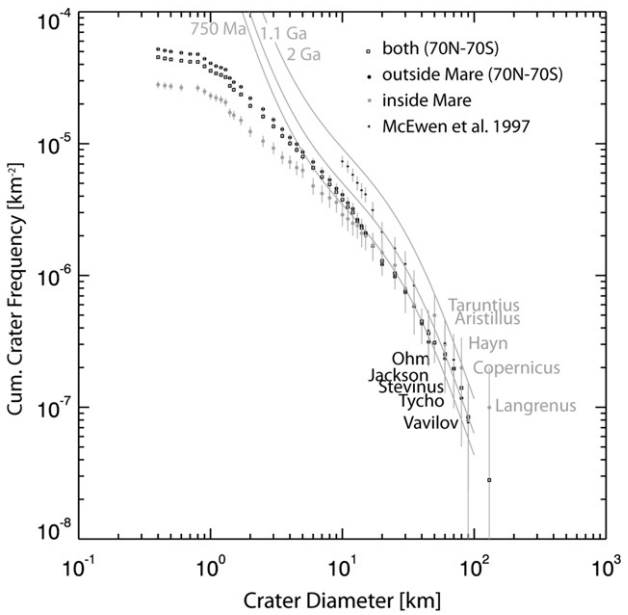


**Fig. 4.** The crater size-frequency distribution of rayed craters inside and outside mare units between 70°N and 70°S latitude in comparison with the total population (Fig. 2). For the mapped mare unit outline compare with Fig. 1. While the larger-sized craters inside mare units appear more abundant, it is opposite for the smaller-size ranges. The total population averages both curves, and the size-frequency distribution naturally plots in between the two separate distributions. For comparison with earlier studies, the farside lunar rayed crater distribution by McEwen et al. (1997) is plotted. Isochrones for average surface ages of 750 Ma and 1.1 Ga (the estimated Eratosthenian–Copernican boundary) and 2 Ga are given.

The crater size-frequency distribution for the area outside the mare units are fitted by an isochrone for an average surface age of 750 Ma (following Ivanov, 2001; Neukum et al., 2001) down to a crater diameter of about 5 km, although slight deviations are observed (Fig. 4). The crater frequency drops below the isochrone at a diameter around 20 km, similar to observations of McEwen et al. (1997). We can assign this deviation to the transition between simple and complex craters, which is at about 21 km diameter for the highlands (Pike, 1981). The highland crater population seems to exceed the isochrone for crater diameters around 10 km in diameter before the curve continues well below the isochrones (for craters of 5 km and smaller in diameter) because of the crater size-dependence of ray maturity (Grier et al., 2001; Hawke et al., 2004). The steepening above the isochrone was already described by McEwen et al. (1997), but is found for the rayed-crater population not to be as pronounced as earlier crater counts suggest (Fig. 4). The crater distribution measured by McEwen et al. (1997) is in general steeper in comparison to isochrones and to the pure rayed-crater population described here.

The mare crater size-frequency distribution appears to be somewhat different from the highland one. For the larger crater size range (larger than 50 km in diameter), craters inside mare units are more abundant compared to the 750-Ma isochrone. The large-crater excess is attributable to the prolonged ray visibility when caused by composition rather than immaturity. In Fig. 5, the mare crater size-frequency distribution for the entire rayed-crater population is plotted and compared to the distribution of the crater population without those for which the ray visibility is due to composition rather than immaturity. Whereas the larger crater population inside mare units appears to exceed the 750 Ma isochrone, it fits well to this isochrone after the compositional rayed craters were removed from the population (following Grier et al., 2001). Extracting large craters from the population results in an increase of the gradient representing the cumulative distribution (compare the discussion on resurfacing treatment by Werner, 2009), and therefore the correlation between observation and isochrone improves. Generally, the distribution at intermediate crater diameters (5 km to 12 km) is better represented by a 650-Ma isochrone (following Ivanov, 2001; Neukum et al., 2001), implying either a comparatively lower crater-production rate for the mare units or more rapid decay in the visibility of rays. The latter is

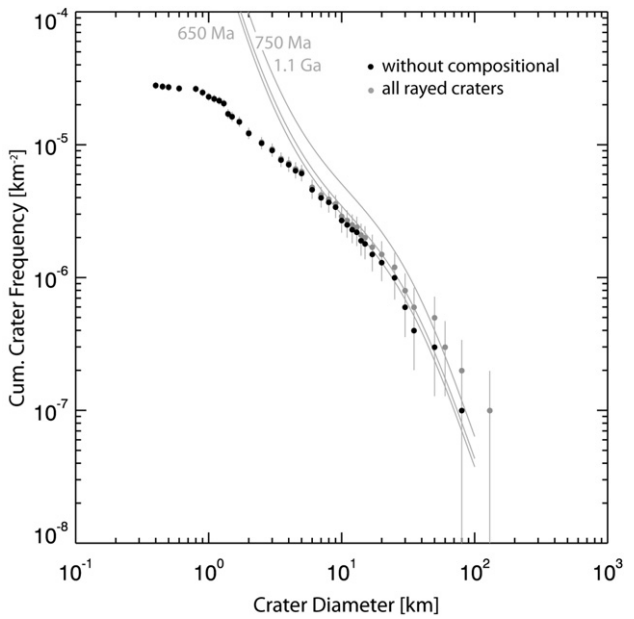


**Fig. 5.** The crater size-frequency distribution of rayed craters inside mare units (Fig. 4), and the same rayed crater population without the craters for which the ray visibility is due to composition rather than immaturity. While the larger crater population inside mare units appears to exceed the isochrone, it is in agreement after the compositional rayed craters were removed from the population. Isochrones for average surface ages of 650 Ma, 750 Ma, and 1.1 Ga (the estimated Eratosthenian–Copernican boundary) are given.

supported by Pieters et al. (1993) who showed that even fresh mare craters, although brighter than the surrounding mare soil, rarely exceed the albedo of typical highland soils, and the brightest spots on the Moon are related to high abundances of plagioclase which are dominantly found in the highland units.

For the smaller crater size range (smaller than 5 km diameter) the crater frequency drops below the isochrone (i.e., the 650-Ma isochrone), because of the crater size-dependence of ray maturity, as observed for highland units. A slight drop in the crater size-frequency distribution around 15 km may be attributed to the simple-to-complex crater transition that is shifted in mare units (Pike, 1981), although disturbed by the general trend of deviation from the isochrone. Allen (1977) demonstrated that with respect to the size-frequency distribution the rayed-crater population is a representative subset of the larger population of fresh-looking craters. We confirm this conclusion by demonstrating good agreement between the rayed-crater population and the shape of the crater-production function (isochrone, Figs. 4 and 5).

The total ray crater population (Fig. 3) is naturally the result of adding both distributions (Fig. 4), which averages both curves weighted by the areal contribution, and lies between the separate mare and highland populations. For studying the spatial crater distribution and eventually variations between the hemispheres, as well as pole–equator and near- and farside, we consider the total population, omitting craters larger than 50 km in diameter.

### 2.3. Side-note on compositional effects on the crater population

The ray detectability is lower in mare units than on highland units, and therefore the population observable in the mare units is depleted. The apparently younger mare crater population reflects compositional differences. Following Noble et al. (2007), the term *space weathering* summarizes the micrometeorite bombardment and the interaction of solar wind and cosmic rays (energetic charged particles) with the surface of atmosphere-less bodies, such as the Moon. It changes the optical properties of the surface so that with time the brightness of the surface decreases while the spectral reddening increases. The process is faster for mare units than highland areas. A possible explanation is that the contrast between fresh and matured soils is already lower (albedo ranges between 7% and 10%) compared to highland soils (albedo ranges between 11% and 18%) and that the process of maturation is accelerated due to the relative iron content, one of the significant compositional differences (Morris, 1976; Allen et al., 1996; Noble et al., 2001).

## 3. Spatial crater distribution — Detectable asymmetries?

The geological difference between mare and highland units does not significantly influence the shape of the crater size-frequency distribution, although a slight tendency towards lower numbers is observed for the mare units compared to highland units. The global distribution of ray craters will be used to investigate spatial asymmetries for the cratering rate on the lunar surface representative for at least the last 750 Ma. The ratio of crater frequencies outside and inside mare units is determined and used to correct the crater numbers in the spatial investigations to avoid biases, especially at the smaller-size range.

The GIS system provides tools to select craters with distance from (for example) the apex or antapex with dependence on size or any other attribute assigned to the crater, such as latitude, longitude or diameter. Consequently, any rayed-crater subset can be defined and compared to the predicted crater-rate asymmetries suggested or discussed by Turski (1962), Halliday (1964), Wiesel (1971), Bandermann and Singer (1973), Wood (1973), Shoemaker and Wolfe (1982), Horedt and Neukum (1984), Zahnle et al. (1998, 2001, 2003), Morota and Furumoto (2003), Morota et al. (2005, 2008), Le Feuvre and Wieczorek (2005, 2006, 2008), Gallant et al. (2009).

In the previous sections we showed that the frequency of craters in mare units is lower than in highland units, and a satisfactory explanation for this difference is yet not found. Possible explanations include global asymmetry of the crater distribution on Moon, or simply the lower detectability of the rays in the mare units. If the latter is the main reason, the global analysis of spatial distribution will be inaccurate. To account for this, we calculate the ratio of the crater frequencies within and outside mare units (Fig. 6). The ratio shows that the small (<5 km in diameter) craters appear in highland units 1.85 times more often than in the mare units. Thus, if we assume that the low detectability of the craters is the reason for lower frequency of the craters in mare units, we have to adjust the numbers of the craters by the ratio of 1.85 in mare areas. The crater range 5–50 km gives an average ratio of frequencies of 1.45. This variance between mare and highland crater size-frequency distribution is evaluated (Fig. 6) and corrected to avoid any bias due to detectability in the spatial investigation.

### 3.1. Latitudinal dependence

The study of the latitudinal dependence aims to explore whether the spatial crater distribution is affected by projectiles mainly moving close to the ecliptic plane. As suggested by Halliday (1964), Le Feuvre and Wieczorek (2006, 2008), Gallant et al. (2009), higher crater frequencies may be expected closer to the equator than to the pole. To test this model prediction, craters were extracted from the database according to latitude using a 30° sized moving-window at steps of 3°. This was done for diameter ranges of 1 to 5 km and 5 to 50 km. The total population behaves similarly to the crater population with diameters between 1 km and 5 km. This is due to the power-law characteristics of the population: $N_{\mathrm{cum}} \sim D^{-b}$, i.e. the population of craters with diameter $D$ and larger is proportional to the diameter in the power of $-b$, and for a cumulative description b ranges between 2 and 3.5 (Ivanov, 2001). Thus, small craters outnumber the large ones by at least a factor of five. Fig. 7A shows results for both sets with and

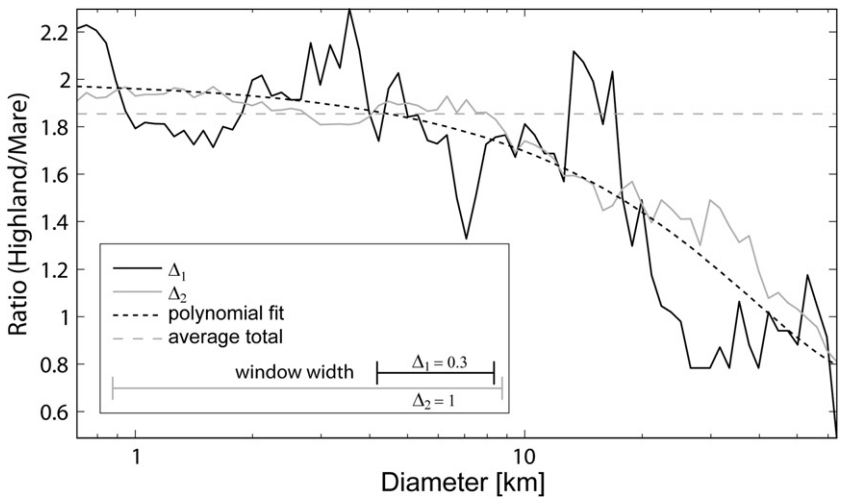


**Fig. 6.** The ratio of crater frequencies outside and within mare units. The two curves (gray and black) are calculated using differently sized moving windows (the window width is constant only in logarithmic scale), but share a similar behaviour. The polynomial fit is used as a measure to correct for the more rapid ray-fading in mare areas when global crater densities are determined (Fig. 9). The average ratio for entire set of craters is 1.85, whereas craters with diameters of 5–50 km give an average of 1.45.

without corrections for mare units. The crater frequencies are normalized according to the average and plotted against latitude, and error bars are shown for the uncorrected crater frequencies. The statistical uncertainties for the corrected crater population are slightly smaller.

In comparing the observed and the predicted normalized density distribution (e.g., Le Feuvre and Wieczorek, 2008), we find the observed deviations to be larger and more random. No clear density pattern is observed for craters with diameters larger than five kilometres. At latitudes around 20°N the frequency drops. This is only marginally related to the lower numbers found in the mare regions, because it remains even after the corrections for lower frequencies in the mare units. The frequency variations for the smaller craters show a trend which is opposite to the one predicted by Le Feuvre and Wieczorek (2008). High crater frequencies are found at high latitudes. The correction for effects of the mare units (dashed line in Fig. 7A) does not change this tendency although a minor reduction of the amplitude of the variations is observed.

### 3.2. Longitudinal dependence

The leading hemisphere of synchronously rotating satellites is expected to be cratered at a higher rate than on the trailing hemisphere (e.g., Shoemaker and Wolfe, 1982; Horedt and Neukum, 1984; Zahnle et al., 1998). This asymmetry results because the orbital velocity of the satellite is large compared to the space velocity of the impactor. The cratering rate asymmetry of the Moon is hence much less than for satellites of, for example, Jupiter. To test if any asymmetry is detectable, crater frequency variations were calculated with angular distance from the apex by using a 30° sized moving-window at steps of 3° for diameter ranges of 1 to 5 km and 5 to 50 km. Fig. 7B shows both distributions with and without corrections for mare units, although in both cases the corrections change neither the amplitude nor the shape of the variations significantly. Errors are shown for the uncorrected crater population. For the small and large crater range low frequencies are found close to the apex followed by a maximum at a distance of about 60° away from the apex. The frequency of larger craters drops at a distance of about 90° and scatter around average on the antapex-hemisphere. The frequency variations for the smaller craters drop to a low at a distance of about 100° from the apex and scatter for the antapex-hemisphere at about 20% below average. No maximum is observed at the apex of the orbital motion (even if 1-sigma uncertainties are considered), but one is observed roughly sixty degrees away. As expected from the observations for the latitudinal variations, where higher frequencies are found at high latitudes and not at the equator (Fig. 7A), the maximum frequency is observed at the distance of about 60° away from the apex (Fig. 7B).

Fig. 8 shows the cumulative crater size-frequency distributions within radii of 15, 30, 45 and 70° distance from the apex of orbital motion in comparison with the equivalent distribution of the antapex side. When comparing absolute values of the crater densities (only for craters below about one kilometre in diameter) the crater densities at the apex exceed the crater densities of similarly sized area at the opposite hemisphere. For a better understanding of the global density distribution, crater-density maps for the lunar surface between 70°N and 70°S were produced (Fig. 9). The densities are shown uncorrected and corrected for different averages within and outside of mare units. The correction values were derived from the total crater distribution (Fig. 6) and are 1.45 for intermediate crater sizes (5–50 km in diameter) and 1.85 for small craters (with diameters between 1 and 5 km). The densities are calculated for a search radius of 30 and 90° at a raster resolution of 1° node distance. The search radii were chosen to characterize hemispherical differences (90° search radius) and more localized descriptions (30° search radius). The density maps derived from the small crater population and from the total crater population are similar because the total population is dominated by the small crater population.

For the 90° search radius density map, an antipodal distribution is apparent, showing a maximum for the leading hemisphere close to the apex. Such a distribution is not as obvious for the large-crater distribution. The correction for the lower numbers inside the mare units results in shifting the maximum of the frequency high of large craters away from the apex position. The hemispherically-averaged density map seems to correlate well in amplitude and spatial distribution with model-predicted distributions. However, when studying the crater densities in less averaging manner by using a

**Fig. 7.** Variations of the normalized crater frequencies of ray craters with latitude (A), angular distance from the apex (B), and angular distance from the nearside point (C) calculated using a 30° sized moving-window (illustrated as light gray area in the cartoons on the right hand side) at steps of 3° for diameter ranges of 1 km to 5 km and 5 km to 50 km in diameter, shown with and without corrections for mare units, and in comparison with an analytical prediction (LeFeuvre and Wieczorek, pers.com.). Transparent ribbons of corresponding colour outline the 1-sigma uncertainties. The corrected distributions have similar or slightly smaller uncertainties.

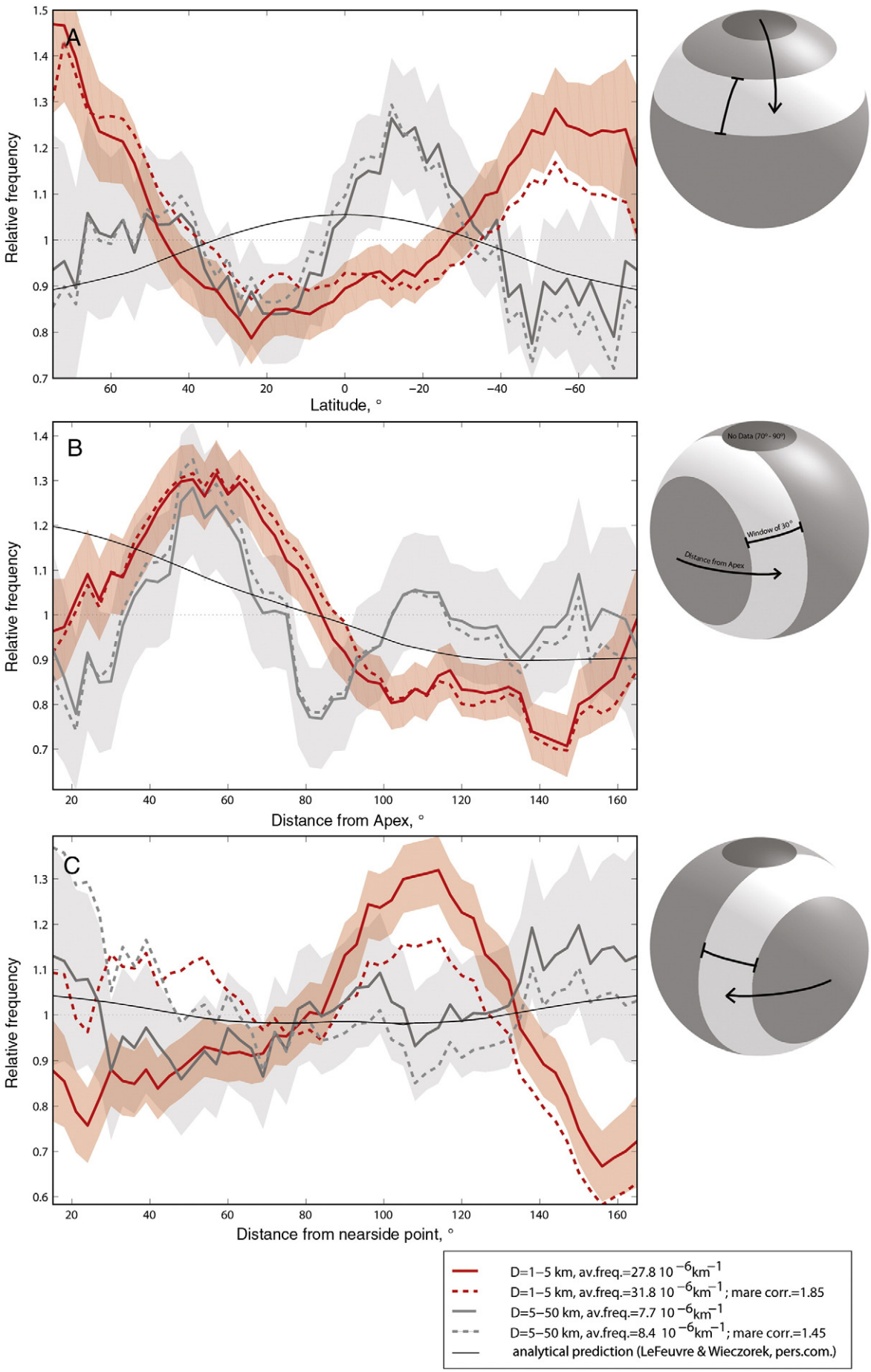

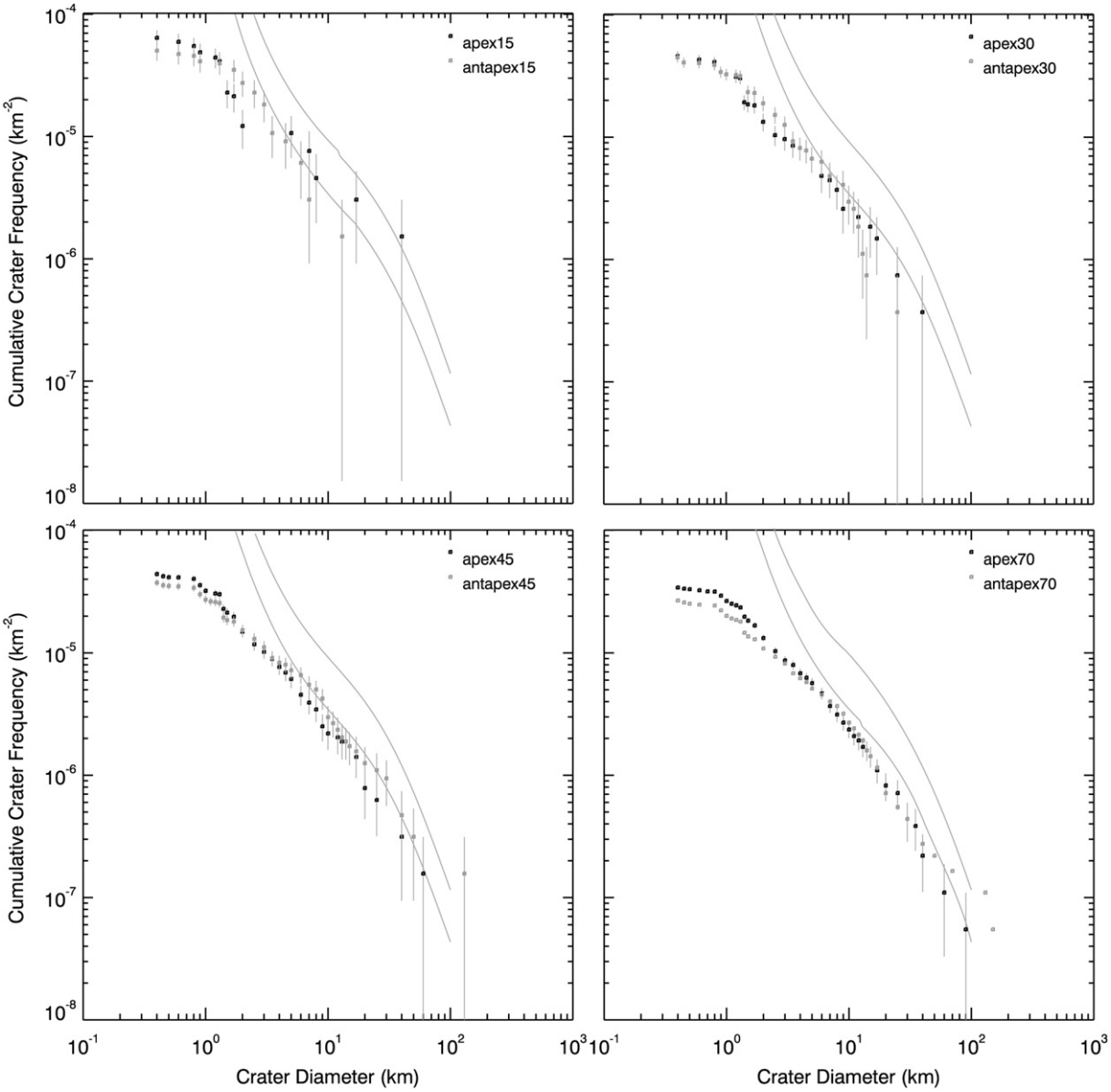


**Fig. 8.** Cumulative size-frequency distribution within 15, 30, 45 and 70° distance from the apex in comparison with the equivalent distribution at the antapex side. Isochrones for average surface ages of 750 Ma and 1.1 Ga (the estimated Eratosthenian–Copernican boundary) are given.

search radius of 30°, the pattern differs significantly. All map derivatives show a more patchy distribution, although corrected for the mare units the density maximum is found rather at high latitudes than near the equator. A dominance at the leading side is still observed, but the apex and its surroundings show relatively lower densities.

### 3.3. Nearside–farside dependence

Whether there is a visible effect between the nearside and the farside, is debated for the Moon (Turski, 1962; Wiesel, 1971; Bandermann and Singer, 1973; Wood, 1973; Le Feuvre and Wieczorek, 2005; Gallant et al., 2009). This effect most likely acts at smaller separations between planet and satellite if the majority of projectiles approach the system with inclination close to the satellite-orbit plane. Fig. 7C shows the observed crater population in comparison with the analytically predicted one. The strongest influence between nearside and farside is the differing composition affecting the detectability of rayed craters. However, the observed population is representative only for very recent impact bombardment so that any emphasizing of a nearside–farside effect due to smaller separation distance would not be detected.

## 4. Discussion and conclusions

Our study of the spatial and size-frequency distribution of rayed craters on the Moon show that spatial asymmetries exist. They do not,

**Fig. 9.** Crater densities for the lunar surface between 70 °N and 70 °S, uncorrected (left) and corrected (right) for different averages within and without mare units. The densities are calculated for a search radius of 30° (upper six panels) and 90° (lower six panels) at a raster resolution of 1° node distance. The density maps are derived for the total crater distribution (first and fourth row), for small craters (with diameters between about 1 km and 5 km in diameter, second and fifth row) and for intermediate crater sizes (5 km–50 km in diameter, third and sixth row).

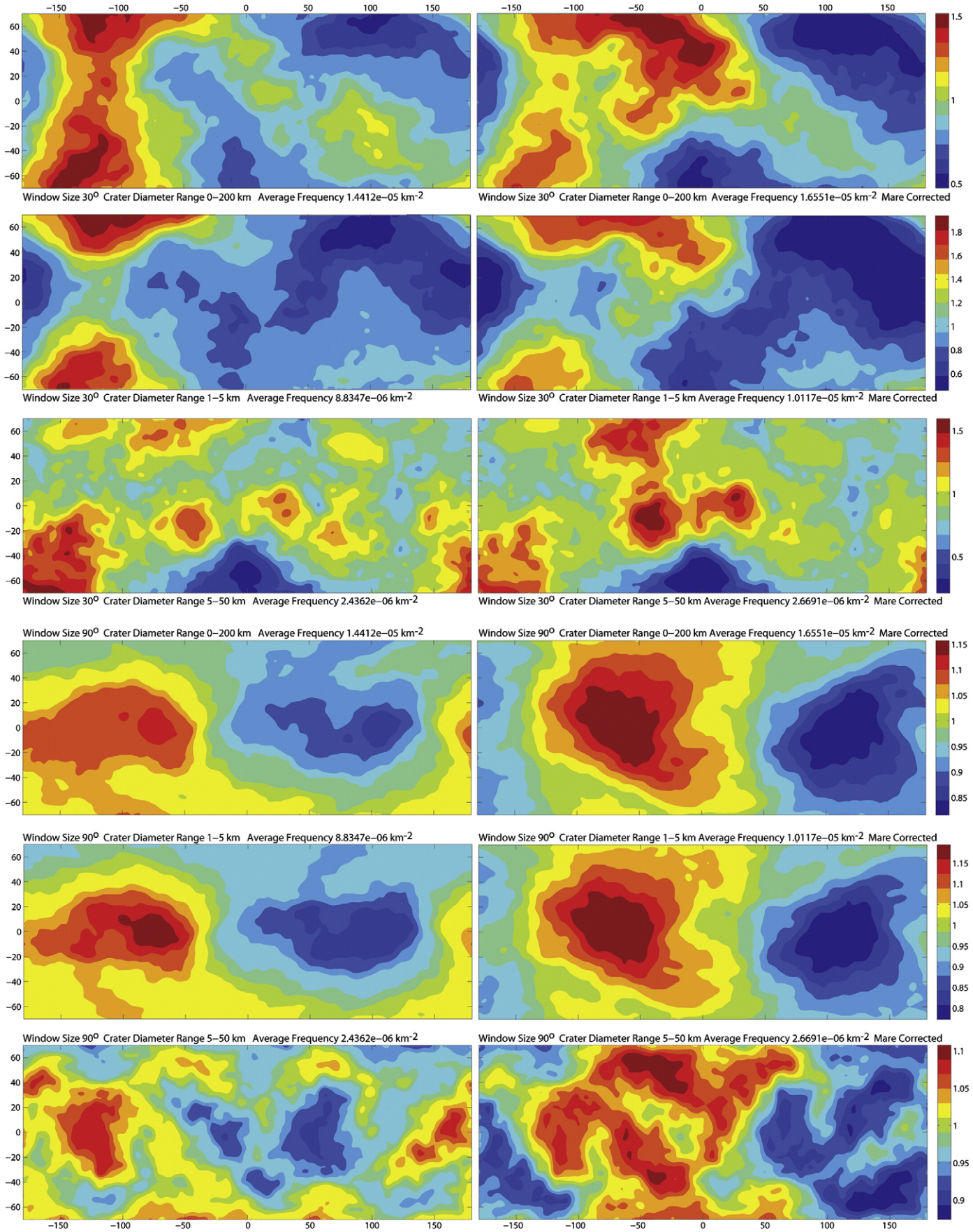

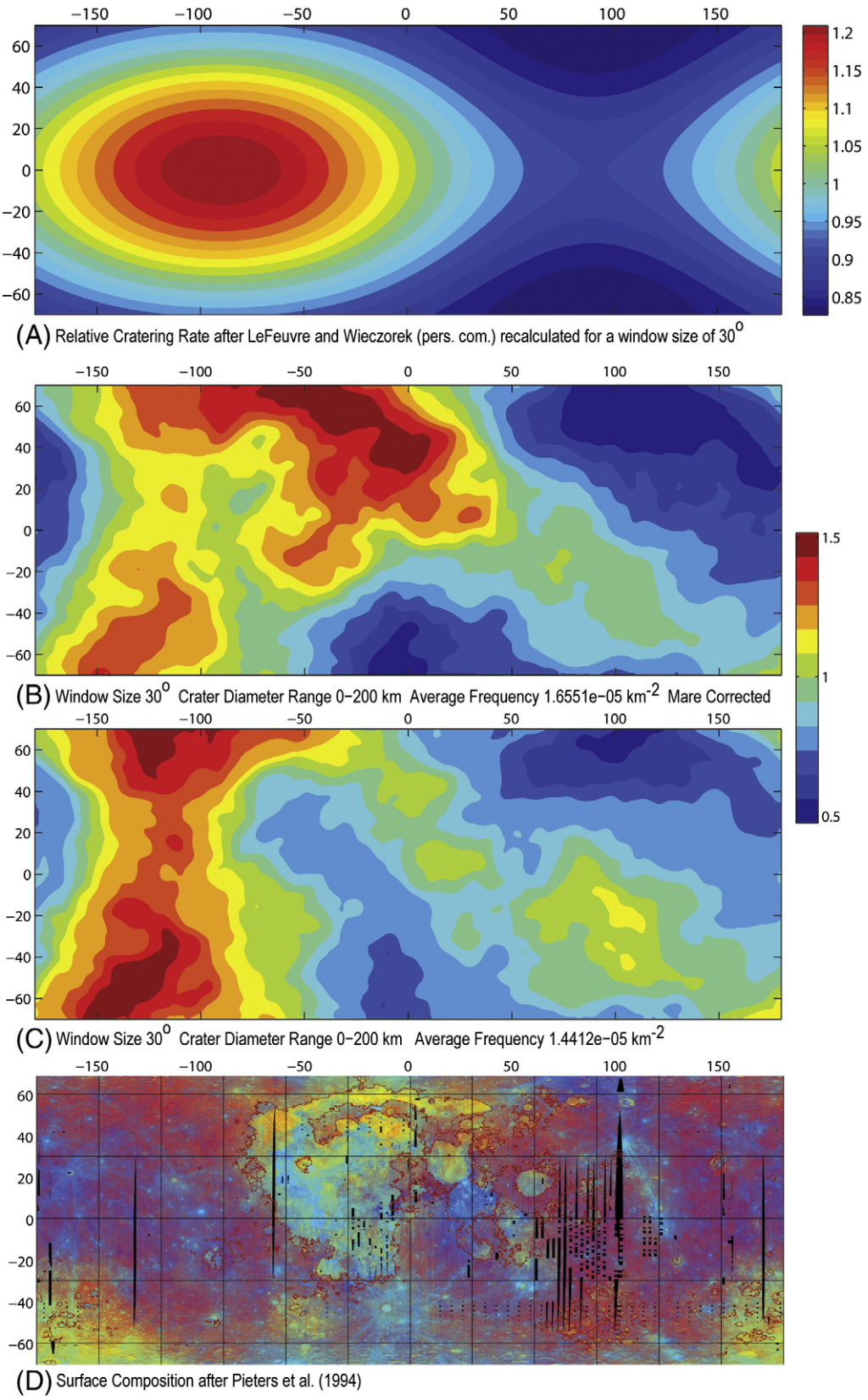


**Fig. 10.** Comparison of the analytically predicted spatial crater distribution (A, after LeFeuvre and Wieczorek, pers.com.), the observed total crater distribution (Fig. 9), which is corrected for lower frequencies in the mare units (B) and uncorrected (C) and an impression of the surface composition (D) as given through mineral-ratio data presented as a RGB composite image mosaic with band ratios 750 nm/415 nm shown in red (R), 750 nm/950 nm in green (G) and 415 nm/750 nm in blue (B), (Pieters et al., 1994).

however, show patterns predicted by models that use the present day orbital configuration of the Moon. The patterns are more complex. Density variations are less than 15% for most of the lunar surface, and the uncertainties for absolute surface ages are similar. However, variations of up to 50% are found even for small and numerous craters. These extreme values are located at high latitudes. Although geological

processes forming the lunar surface do not affect the rayed-crater distribution, the inherited target properties of earlier geological activity or even primordial crustal compositional differences have a strong influence on the ray retention (Fig. 10). We show that the number of small craters exhibiting rayed ejecta in mare units is almost two times lower than in the highland units. A likely explanation for the difference is the accelerated ray obliteration in mare areas because of the higher iron content and lower albedo contrast. This is true only for so-called maturity rays, which fade away due to space weathering, but not if the rays are visible due to compositional differences. Large, old, rayed craters sustain their visibility longer than the average crater population because of compositional contrast between rays and mare material, and thus obscure the cratering record when investigated for spatial variations as predicted from analytical and numerical studies.

The observed spatial crater distribution, which contradicts the predicted crater distribution and shows highest frequencies at the poles instead of near the equator, is puzzling, as there are no obvious compositional variations (Fig. 10) and a recent reorientation of the lunar surface with respect to the spin axis is unlikely (e.g. Wisdom, 2006). However, it could be a result of the predicted cratering rate distribution: a combination of the crater-forming projectile flux and the micrometeorite bombardment. The latter acts on the maturation of the rayed deposits and is, following the predicted pattern, strongest at the leading site and at equatorial latitudes. Therefore, the ray removal is enhanced at a similar global pattern, and the apparently contradictory spatial crater distribution pattern is amplified. Looking at the smaller-sized crater population, the deviation is more pronounced (Fig. 7A and B), and in agreement with the observation, that rays of smaller craters disappear faster than for larger ones (Fig. 2).Hawke et al. (2004) suggested to use the existence of rays purely based on optical maturity instead of visibility as marker horizon for the Copernican–Eratosthenian boundary, implying that a number of craters mapped as Copernican need reassignment (Hawke et al., 2008). The absolute age isochrone marking the ray retention time is subject to uncertainties within the cratering chronology calibration, such as the assumption of a temporally constant cratering rate. However, radiometric ages are in good agreement with the ages derived using cratering statistics. The total rayed-crater population is represented well by the 750 Ma isochrone (following Ivanov, 2001; Neukum et al., 2001). This implies that the ray retention time even for large craters is approximately 750 Ma or less, and could be the revised age value for the Copernican–Eratosthenian boundary. Analysis of the older craters would be even more complicated (at least on the Moon) because early geological processes disturb the situation and the orbital configurations of the Moon–Earth–Sun–projectile system are less known.

## Acknowledgements

We thank M. LeFeuvre and two anonymous reviewers for the questions and suggestions, which improved the earlier version of the manuscript. This work was supported by the Norwegian Research Council through a Centre of Excellence grant to PGP.

## References

Allen, C.C., 1977. Rayed craters on the Moon and Mercury. Phys. Earth Planet. In. 15, 179–188.
Allen, C.C., Morris, R.V., McKay, D.S., 1996. An experimental analog to maturing lunar soil. 27th Lunar and Planetary Science Conference, pp. 13–14.
Bandermann, L.W., Singer, S.F., 1973. Calculation of meteoroid impacts on Moon and Earth. Icarus 19, 108–113.
Blewett, D.T., Hawke, B.R., 2001. Remote sensing and geological studies of the Hadley–Apennine region of the Moon. Meteorit. Planet. Sci. 36 (5), 701–730.
Crater Analysis Techniques Working Group: Arvidson, R.E., Boyce, J., Chapman, C., Cintala, M., Fulchignoni, M., Moore, H., Neukum, G., Schultz, P., Soderblom, L., Strom, R., Woronow, A., Young, R., 1979. Standard techniques for presentation and analysis of crater size-frequency data. Icarus 37, 467–474.
Gallant, J., Gladman, B., Ćuk, M., 2009. Current bombardment of the Earth–Moon system: emphasis on cratering asymmetries. Icarus 202 (2), 371–382.
Grier, J.A., McEwen, A.S., Lucey, P.G., Milazzo, M., Strom, R.G., 2001. Optical maturity of ejecta from large rayed lunar craters. J. Geophys. Res. 106, 32847–32862.
Halliday, I., 1964. The variation in the frequency of meteorite impact with geographic latitude. Meteoritics 2 (3), 271–278.
Hartmann, W.K., 1966. Early lunar cratering. Icarus 5, 406–418.
Hawke, B.R., Blewett, D.T., Lucey, P.G., Smith, G.A., Bell III, J.F., Campbell, B.A., Robinson, M.S., 2004. The origin of lunar crater rays. Icarus 170, 1–16.
Hawke, B.R., Giguere, T.A., Gaddis, L.R., Campbell, B.A., Blewett, D.T., Boyce, J.M., Gillis-Davis, J.J., Lucey, P.G., Peterson, C.A., Robinson, M.S., Smith, G.A., 2008. The origin of Copernicus Rays: implications for the calibration of the lunar stratigraphic column. 39th Lunar and Planetary Science Conference No. 1391.
Hiesinger, H., Head III, J.W., Wolf, U., Jaumann, R., Neukum, G., 2003. Ages and stratigraphy of mare basalts in Oceanus Procellarum, Mare Nubium, Mare Cognitum, and Mare Insularum. J. Geophys. Res. 108 (E7), 5065. doi:10.1029/2002JEOO1985.
Horedt, G.P., Neukum, G., 1984. Cratering rate over the surface of a synchronous satellite. Icarus 60, 710–717.
Ivanov, B., 2001. Mars/Moon cratering rate ratio estimates. Space Sci. Rev. 96, 87–104.
Le Feuvre, M., Wieczorek, M.A., 2005. The asymmetric cratering history of the moon. 36th LPSC abstract no.2043.
Le Feuvre, M., Wieczorek, M.A., 2006. The asymmetric cratering history of the terrestrial planets: latitudinal effect. 37th LPSC abstract no.1841.
Le Feuvre, M., Wieczorek, M.A., 2008. Nonuniform cratering of the terrestrial planets. Icarus 197, 291–306.
Lucchitta, B.K., 1978. Geologic Map of the North Side of the Moon. USGS I-1062, NASA.
Lucey, P.G., Blewett, D.T., Jolliff, B.L., 2000a. Lunar iron and titanium abundance algorithms based on final processing of Clementine UV–VIS data. J. Geophys. Res. 105, 20297–20305.
Lucey, P.G., Blewett, D.T., Taylor, G.J., Hawke, B.R., 2000b. Imaging of lunar surface maturity. J. Geophys. Res. 105, 20377–20386.
McCord, T.B., Charette, M.P., Johnson, T.V., Lebofsky, L.A., Pieters, C., Adams, J.B., 1972a. Lunar spectral types. J. Geophys. Res. 77 (8), 1349–1359.
McCord, T.B., Charette, M.P., Johnson, T.V., Lebofsky, L.A., Pieters, C., 1972b. Spectrophotometry (0.3 to 1.1 μ) of visited and proposed Apollo lunar landing sites. Moon 5, 52–89.
McEwen, A.S., Moore, J.M., Shoemaker, E.M., 1997. The Phanerozoic impact cratering rate: evidence from the farside of the Moon. J. Geophys. Res. 102, 9231–9242.
Morota, T., Furumoto, M., 2003. Asymmetrical distribution of rayed craters on the Moon. Earth Planet. Sci. Lett. 206, 315–323.
Morota, T., Ukai, T., Furumoto, M., 2005. Influence of the asymmetrical cratering rate on the lunar chronology. Icarus 173, 322–324.
Morota, T., Haruyama, J., Furumoto, M., 2008. Lunar apex–antapex cratering asymmetry and origin of impactors in the Earth–Moon system. Adv. Space Res. 42, 285–288.
Morris, R., 1976. Surface exposure indices of lunar soils — a comparative FMR study. 7th Lunar Science Conference Proceedings. 1, pp. 315–335.
Neukum, G., 1983. Meteoritenbombardement und Datierung planetarer Oberflächen. Habilitation Dissertation for Faculty Membership, Ludwig-Maximilians-University Munich. 186 pp.
Neukum, G., Ivanov, B.A., Hartmann, W.K., 2001. Cratering records in the inner solar system in relation to the lunar reference system. Space Sci. Rev. 96 (1/4), 55–86.
Noble, S.K., Pieters, C.M., Taylor, L.A., Morris, R.V., Allen, C.C., McKay, D.S., Keller, L.P., 2001. The optical properties of the finest fraction of lunar soil: Implications for space weathering. Meteorit. Planet. Sci. 36 (1), 31–42.
Noble, S.K., Pieters, C.M., Keller, L.P., 2007. An experimental approach to understanding the optical effects of space weathering. Icarus 192, 629–642.
Oberbeck, V.R., Quaide, W.L., Arvidson, R.E., Aggarwal, H.R., 1977. Comparative studies of Lunar, Martian, and Mercurian craters and plains. J. Geophys. Res. 82, 1681–1698.
Pieters, C.M., Adams, J.B., Mouginis-Mark, P.J., Zisk, S.H., Smith, M.O., Head, J.W., McCord, T.B., 1985. The nature of crater rays: the Copernicus example. J. Geophys. Res. 90, 12393–12413.
Pieters, C.M., Head, J.W., Sunshine, J.M., Fischer, E.M., Murchie, S.L., Belton, M., McEwen, A., Gaddis, L., Greeley, R., Neukum, G., Jaumann, R., Hoffmann, H., 1993. Crustal diversity of the Moon: compositional analyses of Galileo Solid State Imaging Data. J. Geophys. Res. 98 (E9), 17127–17148.
Pieters, C.M., Staid, M.I., Fischer, E.M., Tompkins, S., He, G., 1994. A sharper view of impact craters from Clementine data. Science 266, 1844–1848.
Pike, R.J., 1981. Target-Dependence of Crater Depth on the Moon. 12th Lunar and Planetary Institute Science Conference Abstracts, pp. 845–847.
Ryder, G., Bogard, D., Garrison, D., 1991. Probable age of Autolycus and calibration of lunar stratigraphy. Geology 19, 143–146.
Scott, D.H., McCauley, J.F., West, M.N., 1977. Geologic map of the West Side of the Moon. USGS I-1034, NASA.
Shoemaker, E.M., Hackman, R.J., 1962. Stratigraphic Basis for a Lunar Time Scale. In: Kopal, Z., Mikhailov, Z.K. (Eds.), The Moon; IAU Symposium 14 Academic Press, pp. 289–300.
Shoemaker, E.M., Wolfe, R.A., 1982. Cratering timescales for the Galilean satellites. In: Morrison, D. (Ed.), Satellites of Jupiter. Univ. of Arizona Press, Tucson., pp. 277–339.
Shoemaker, E.M., Hackman, R.J., Eggleton, R.E., 1963. Interplanetary correlation of geologic time. Adv. Astronaut. Sci. 8, 70–89.
Simon, S.B., Papike, J.J., Laul, J.C., 1982. The Apollo 14 regolith — petrology of cores 14210/14211 and 14220 and soils 14141, 14148, and 14149. 13th Lunar and Planetary Science Conference Proceedings. Part 1. (A83-15326 04-91), pp. A232–A246.
Stöffler, D., Ryder, G., 2001. Stratigraphy and isotope ages of lunar geologic units: chronological standard for the inner solar system. Space Sci. Rev. 96 (1/4), 9–54.

Stöffler, D., Ostertag, R., Borchardt, R., Malley, J., Rehfeldt, A., Reimold, W.U., 1982. Distribution and provenance of lunar highland rock types at North Ray Crater, Apollo 16. 12th Lunar and Planetary Science Conference Proceedings. Section 1. (A82-31677 15-91), pp. 185–207.
Stuart-Alexander, D.E., 1978. Geologic Map of the Central Far Side of the Moon. USGS I-1047, NASA.
Turski, W., 1962. On the origin of lunar maria. Icarus 1 (1–6), 170–172.
Werner, S.C., 2009. The global martian volcanic evolutionary history. Icarus 201, 44–68.
Wiesel, W., 1971. The meteorite flux at the lunar surface. Icarus 15, 373–383.
Wilhelms, D.E., 1987. The Geologic History of the Moon: USGS Prof. Paper, 1348.
Wilhelms, D.E., El-Baz, F., 1977. Geologic Map of the East Side of the Moon. USGS I-948, NASA.
Wilhelms, D.E., McCauley, J.F., 1971. Geologic Map of the Near Side of the Moon. USGS I-703, NASA.
Wilhelms, D.E., Oberbeck, V.R., Aggarwal, H.R., 1978. Size-frequency distribution of primary and secondary lunar impact craters. Proc. 9th Lunar Planet. Sci. Conf, pp. 3735–3762.
Wilhelms, D.E., Howard, K.A., Wilshire, H.G., 1979. Geologic Map of the South Side of the Moon. USGS I-1162, NASA.
Wisdom, J., 2006. Dynamics of the lunar spin axis. Astron. J. 131, 1864–1871.
Wood, J.A., 1973. Bombardment as a cause of the lunar asymmetry. Earth Moon Planet. 8, 73–103.
Zahnle, K., Dones, L., Levison, H.F., 1998. Cratering rates on the Galilean satellites. Icarus 136, 202–222.
Zahnle, K., Schenk, P., Sobieszczyk, S., Dones, L., Levison, H.F., 2001. Differential cratering of synchronously rotating satellites by ecliptic comets. Icarus 153, 111–129.
Zahnle, K., Schenk, P., Levison, H., Dones, L., 2003. Cratering rates in the outer Solar System. Icarus 163 (2), 263–289.